PULSE SHAPE
DISCRIMINATOR

Model 2160 A
Operating Manual

FAST ComTec GmbH · Grünwalder Weg 28a · D-82041 Oberhaching · Germany
Tel 49-(0)89-66 51 80 50 · FAX 49-(0)89-66 51 80 40 · http://www.fastcomtec.com

NUCLEAR INSTRUMENTS AND METHODS 116 (1974) 55–59; © NORTH-HOLLAND PUBLISHING CO.

A simple pulse-shape discrimination circuit is described. Some results are presented for NE213 organic liquid scintillators of different sizes.

The influence of the lower threshold energy and the effect of high counting rates on the pulse-shape discrimination properties are shown. Complete rejection of gammas is obtained for a small scintillator (2″ diam. × 1″) even for electron energies down to 0.2 MeV.

1. Introduction

The purpose of this paper is to demonstrate the versatility of a simple pulse-shape discrimination circuit (PSD) to suppress gamma rays in neutron-detection systems utilizing organic scintillators. The method used here is somewhat similar to the zero-crossing circuits published previously[1–5]). The main advantages of this method are its large dynamic range (> 1:100) and the feasibility of quickly checking system capabilities with minimum adjustment. Furthermore, the degree of gamma rejection can be determined and reproduced in a simple and straightforward manner. Our circuit was especially designed for use at the neutron time-of-flight facility[6]) at the Munich MP tandem accelerator where the neutron energies of interest range from 0.5 MeV to about 30 MeV. In our system we use the anode pulse of the photomultiplier for the neutron–gamma discrimination.

2. Principle of operation

Fig. 1 shows the block diagram of the circuit. The anode pulse of the photomultiplier (PM) is integrated and differentiated in a preamplifier A1 so that the zero-crossing point of the output pulse is determined by the fall time of the input pulse. The shaped signal is then fed to a high-gain limiting amplifier A2. The separation of the zero-crossing points corresponding to gammas or neutrons is now greatly enhanced (fig. 2). The overlap of the amplifier signal and the strobe pulse is formed in a gate G. If the strobe signal is placed between the crossing points of gamma and neutron pulses (fig. 2a) only pulses caused by neutrons will produce an output pulse. In our set-up the strobe signal is triggered by the output pulse of a constant fraction trigger[7]) (CFT), which is delayed and stretched in D.

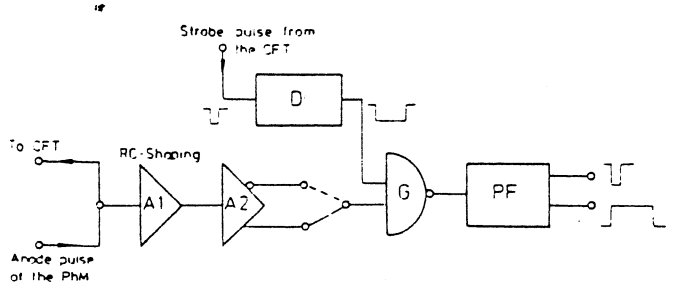

Fig. 1. Block diagram of the circuit.

3. Adjustment procedure

To adjust the unit the inverted output of A2 is used (fig. 2b). The time relation of the gamma and neutron pulses at the output of the PSD unit (in strobe position 1) can be monitored with a time-to-amplitude converter (TAC) (start signal from the CFT, stop signal from the PSD) and a multichannel analyser (fig. 2b). Since the strobe delay is variable, the gamma-rejection ratio can be adjusted (strobe position 2). The onset of the strobe signal appears as a sharp "needle" in the time spectrum since the gate has already been opened by a gamma signal.

After determining the discrimination point the gate input is switched back to the non-inverted output of A2 (fig. 2a). The positive output signal is derived 300 ns after the input pulse.

4. Circuit details

Basically the shaping amplifier consists of an RC integrator followed by an active pole-zero compensated differentiator, i.e. differentiation is performed in the feedback loop of the amplifier (fig. 3). This provides

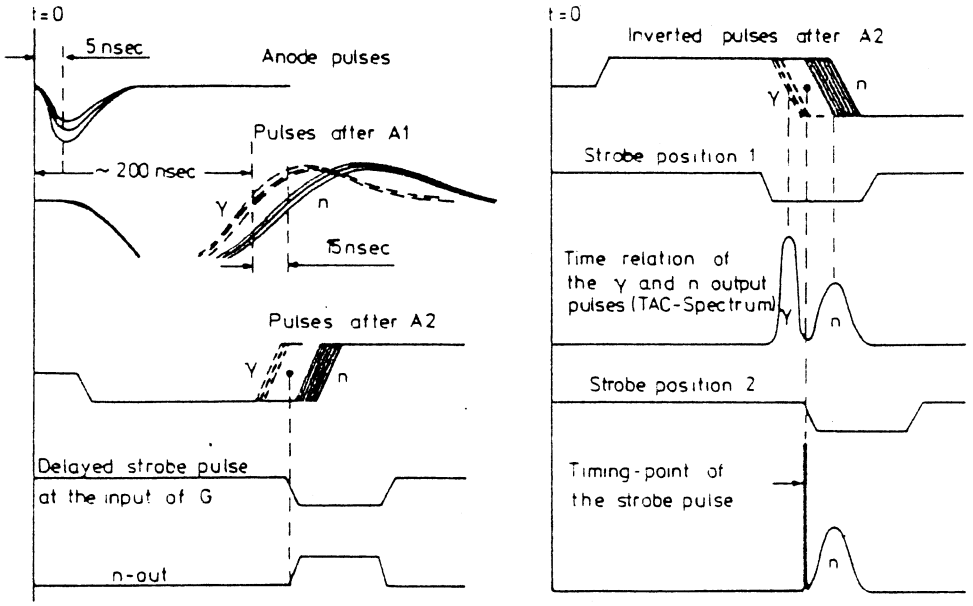

Fig. 2. Time relationship between the pulses at various points of the PSD circuit. a) Normal operation, b) during adjustment.

good isolation between the two shaping networks. High count rate capability and good overload characteristics are major design criteria in this stage. The circuit is therefore dc coupled throughout. Good overload performance is achieved by using a differential pair biased from a constant current source in the input stage. This stage is followed by a class A pre-driver which is in turn coupled to a class AB complementary bipolar output stage. The feedback loop is closed by returning the output via the shaping network to the second input of the differential input stage.

A cascode circuit was chosen for the input half of the differential pair to minimize Miller capacitance at the input of the amplifier. This is important because Miller capacitance at the input is also determined by stray capacitance at the output of the stage which can change appreciably due to minute flexing of the circuit board or of the sides of the NIM cassette. The change in input capacitance alters the integration time constant leading to a corresponding shift of the zero-crossing point: The cascode input circuit makes the mechanical requirements in this respect less stringent and contributes significantly to the long-term stability of the unit.

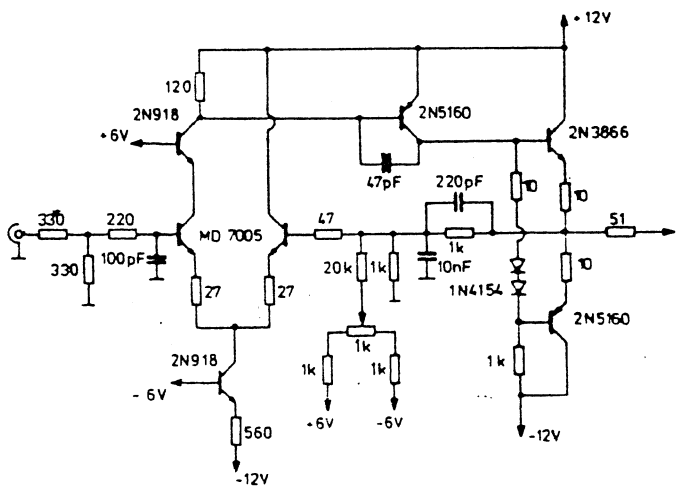

Fig. 3. Circuit diagram of the preamplifier stage.

The balanced bridge type operation of the circuit ensures a stable dc level at the output of the amplifier. Use of a dual transistor for the differential pair takes care of thermal tracking problems which would give rise to a drift in the dc output level. An offset voltage is applied at the feedback input to adapt the dc output level to the input bias requirements of the high-gain limiting amplifier.

It is of the utmost importance that this stage be extremely "clean" and free of spurious responses at all input levels. We therefore carefully checked the open loop response and also performed extensive measurements with both sine wave and pulse inputs.

The fast limiting amplifier (A2, fig. 4) consists of the three cascaded differential amplifier stages of an MC 1065. To increase the dynamic range the supply voltages V_{CC1} and V_{CC2} [8]) are connected to +6 V and +0.8 V respectively. The three stages of the MC 1065 have a double-ended voltage gain of about 10^3. The risetime of the trailing edges of the gamma and neutron pulses (see fig. 2) at the output of the amplifier is about

PULSE-SHAPE DISCRIMINATION CIRCUIT

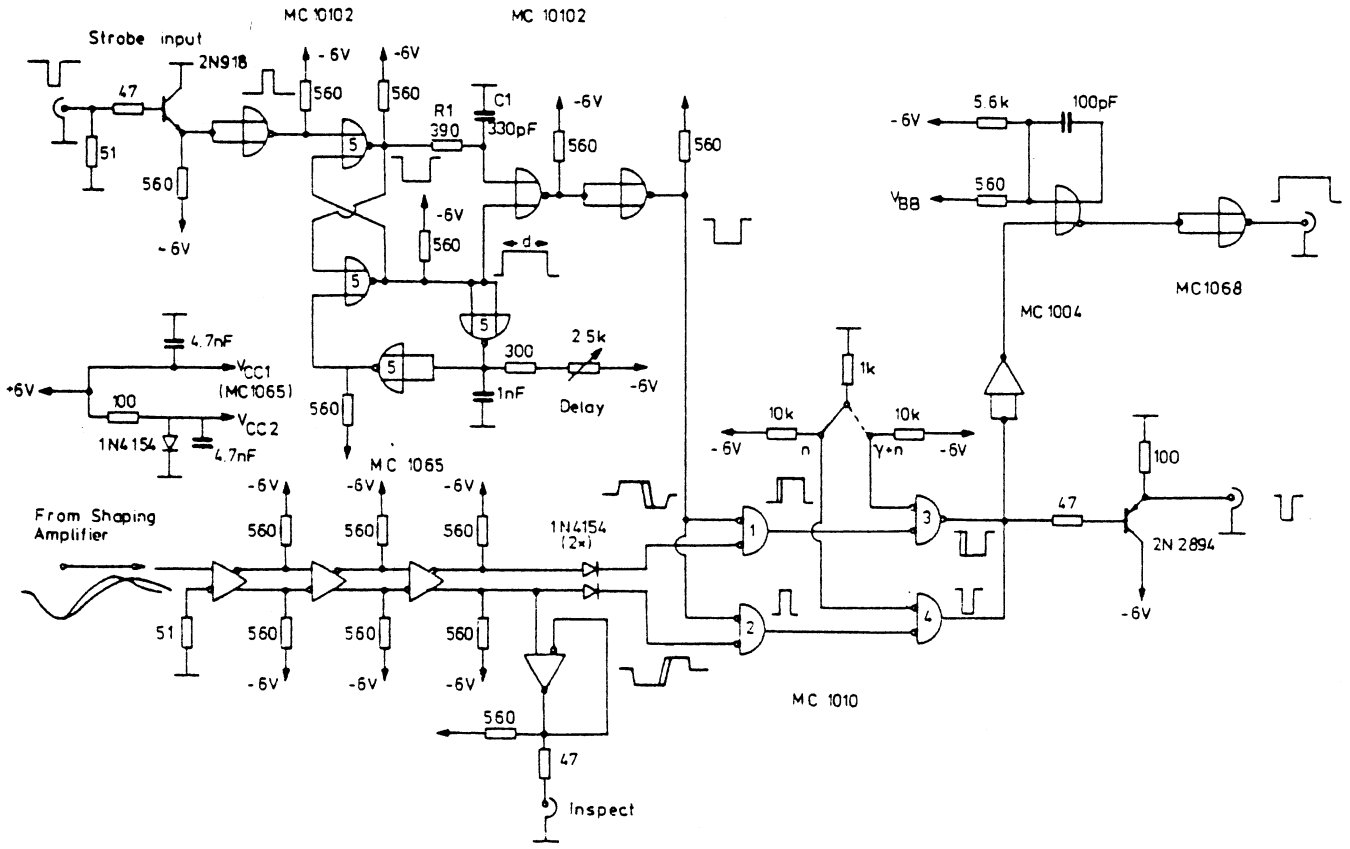

Fig. 4. Pulse shape discrimination circuit – high gain amplifier and strobe circuit.

4 ns. To monitor the amplifier output a unity-gain amplifier (one stage of an MC 1065) is included. This is convenient for adjustment of the dc offset so that the baseline at the output of the limiting amplifier lies in the middle of the output range. The normal and the inverted pulses of A2 are fed together with the split strobe-signal in two NAND-enable gates (each one a quarter of an MC 1010) (IC 1 and IC 2). The leading edge of the output is always defined by the pulse which comes last, provided both pulses overlap.

The gate output derived from either the inverted (IC 1) or non-inverted output (IC 2) of the limiting amplifier can be selected by switching between the two wired-or connected NAND-gates (IC 3 and IC 4).

The negative going output of the MC 1010 stages is translated from MECL levels to fast NIM compatible levels by an emitter-follower. The output of the selector gates is also fed to a simple one-shot (MC 1004) which drives a MECL-to-TTL translator to provide a NIM standard pulse for slow logic applications.

After being translated to MECL levels[8]) the output of the CFT drives a one-shot (IC 5) which generates a pulse of width d. The inverted output of the one-shot is in effect delayed by the integrator R_1C_1 and combined with the non-inverted output in a NOR gate. The output of this gate yields a pulse whose width is defined by R_1C_1 and which is delayed by the time d relative to the input of the one-shot.

The whole circuit is built on a printed circuit board with a ground plane on one side and fits easily into a single width NIM module. The three stages A1, A2 and the strobe circuit are well separated on the board. Great care must also be taken in decoupling the dc-supply voltages between the stages to avoid cross-talk which may give rise to spurious oscillations.

5. Results

The measurements were performed with a 100 mCi Am–Be source filtered by 3 mm of lead in order to reduce the intense 60 keV gamma radiation. An NE213* organic liquid scintillator was used because of its good pulse shape characteristics[9]). The neutron–gamma discrimination properties of the unit were tested using different scintillator sizes. The results obtained with a small scintillator (2″ diam. × 1″) mounted on an RCA 8850 PM tube are given in fig. 5. A clear separation of the neutron and gamma distri-

* NE-Nuclear Enterprises, Edinburgh, Scotland.

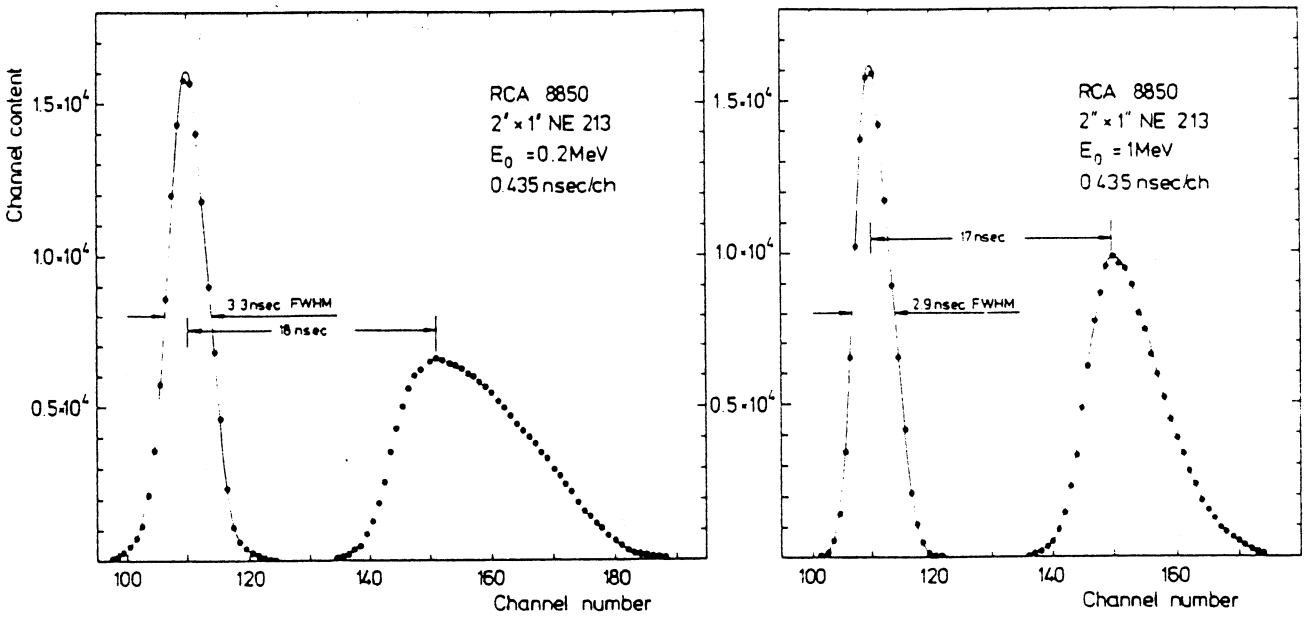

Fig. 5. Neutron–gamma timing distributions with a small scintillator (2" diam. × 1") for two threshold energies.

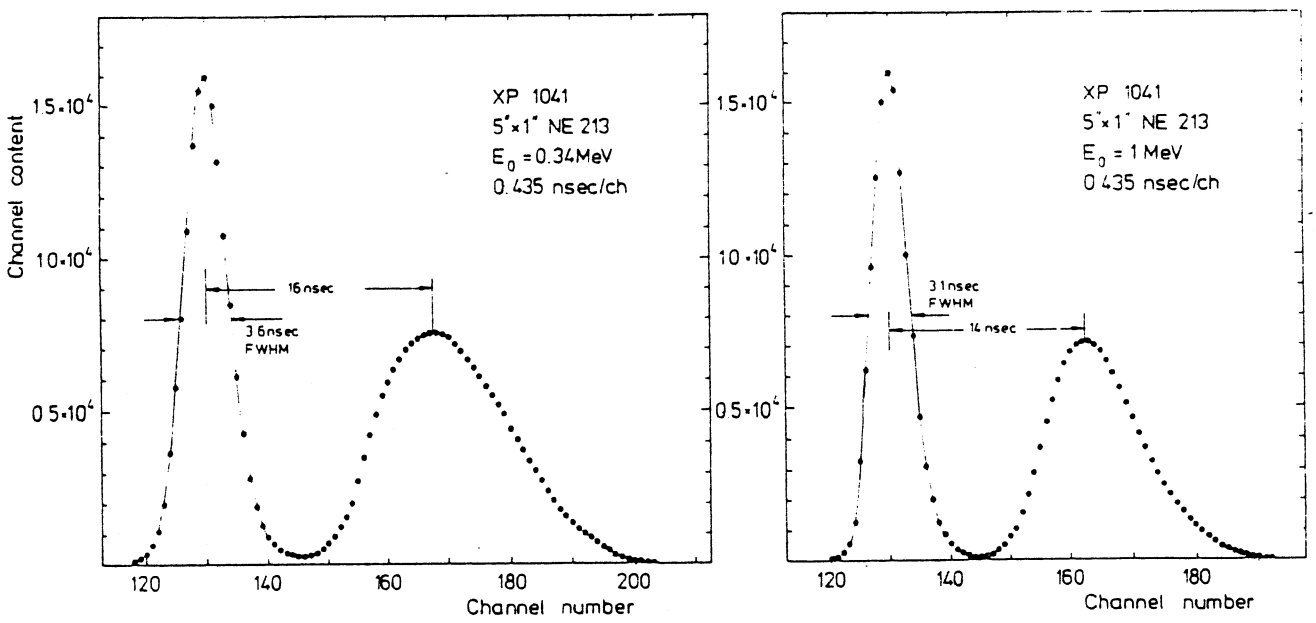

Fig. 6. Neutron–gamma timing distributions with a 5" diam. × 1" scintillator for two threshold energies.

butions is obtained. The gamma peak-to-valley ratio is 1:350 for a lower threshold $E_0 = 0.2$ MeV and shows no strong dependence on energy (1:450 for $E_0 = 1$ MeV). The counting rate in both cases was about 3 kHz. Here and in the following all threshold energies correspond to electron energies.

Other authors[10,11]) have tried to characterize their system capabilities by defining a figure of merit

$$M = \frac{\text{(peak separation)}}{(\gamma \text{ peak width}) + (\text{neutron peak width})}.$$

This is reasonable for strictly Gaussian distributions where the peak-to-valley ratio is implicitly defined by the peak widths and the peak separation. In reality the neutron peak exhibits an energy dependent asymmetry so that M is a rather specious quantity giving no meaningful indication of gamma–neutron discrimination.

The PSD properties with larger scintillators are given in fig. 6. A 5" diam. × 1" NE213 scintillator mounted on an XP 1041 PM tube was used. The peaks for gammas and neutrons are somewhat broadened and the gamma

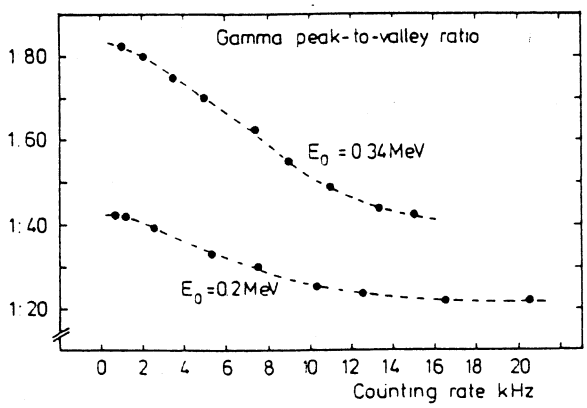

Fig. 7. Counting rate dependence of the gamma peak-to-valley ratio for two lower energy thresholds.

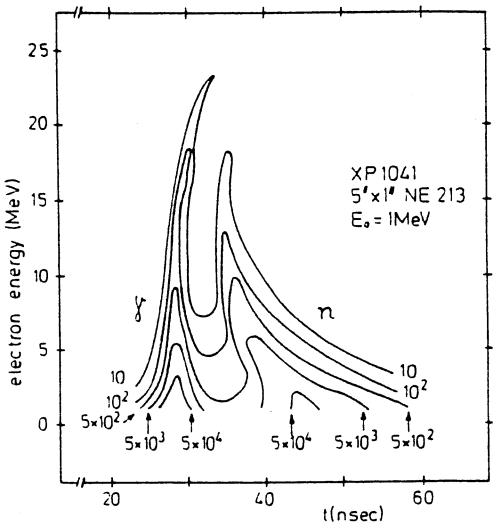

Fig. 8. Contour plot of a two-parametrical neutron–gamma timing distribution vs energy obtained in a $^{26}Mg(^3He, n)^{28}Si$ experiment at $E_{(^3He)} = 18$ MeV.

peak-to-valley ratio shows a stronger dependence on the threshold energy. At about 5 kHz counting rate the peak-to-valley ratio is 1:70 for $E_0 = 0.34$ MeV and 1:120 for $E_0 = 1$ MeV. These values improve for lower counting rates (see fig. 7). The time distributions are well separated and for $E_0 = 1$ MeV a gamma-rejection ratio of 1:1000 without losing neutrons is obtained.

The dependence of the gamma peak-to-valley ratio on the counting rate (for two lower energy thresholds) is given in fig. 7. The indicated counting rates refer to the strobe-signal. The shapes of the gamma and neutron peaks remain the same for all counting rates. Only the valley between them fills up due to pile-up effects which distort the form of the input pulses.

Fig. 8 shows a contour plot of a two parametrical neutron–gamma timing distribution versus energy obtained in a $^{26}Mg(^3He, n)^{28}Si$ experiment at $E_{(^3He)} = 18$ MeV. Gammas and neutrons are clearly separated even for neutron energies up to 27 MeV. The bending of the gamma distribution at higher energies (>20 MeV) into the neutron region is due to saturation effects in the photomultiplier tube.

References

1) T. K. Alexander and F. S. Goulding, Nucl. Instr. and Meth. **13** (1961) 244.
2) M. L. Roush, M. A. Wilson and W. F. Hornyak, Nucl. Instr. and Meth. **31** (1964) 112.
3) C. M. Cialella and J. A. Devanney, Nucl. Instr. and Meth. **60** (1968) 269.
4) T. G. Miller, Nucl. Instr. and Meth. **63** (1968) 121.
5) D. A. Gedcke and C. W. Williams, *High resolution time spectrometry* (Ortec, 1968).
6) K. Rudolph, W. Wieczorek, D. Evers, S. J. Skorka and P. Sperr, to be published.
7) M. R. Maier and P. Sperr, Nucl. Instr. and Meth. **87** (1970) 13.
8) For details of the internal circuitry of the IC's refer to the data sheet of the Motorola MC series.
9) F. T. Kuchnir and F. J. Lynch, IEEE Trans. Nucl. Sci. NS-**15**, no. 3 (June 1968) 107.
10) R. A. Winyard, J. E. Lutkin and G. W. McBeth, Nucl. Instr. and Meth. **95** (1971) 141.
11) R. A. Winyard and G. W. McBeth, Nucl. Instr. and Meth. **98** (1972) 525.

DRAWING NO. B-20177 REV.

REV	CHANGE	ECN	BY	DATE	APPD
	INITIAL RELEASE	3595	RA-	10-7-83	

Date 30.7.83

2160 A

PULSE SHAPE DISCRIMINATOR

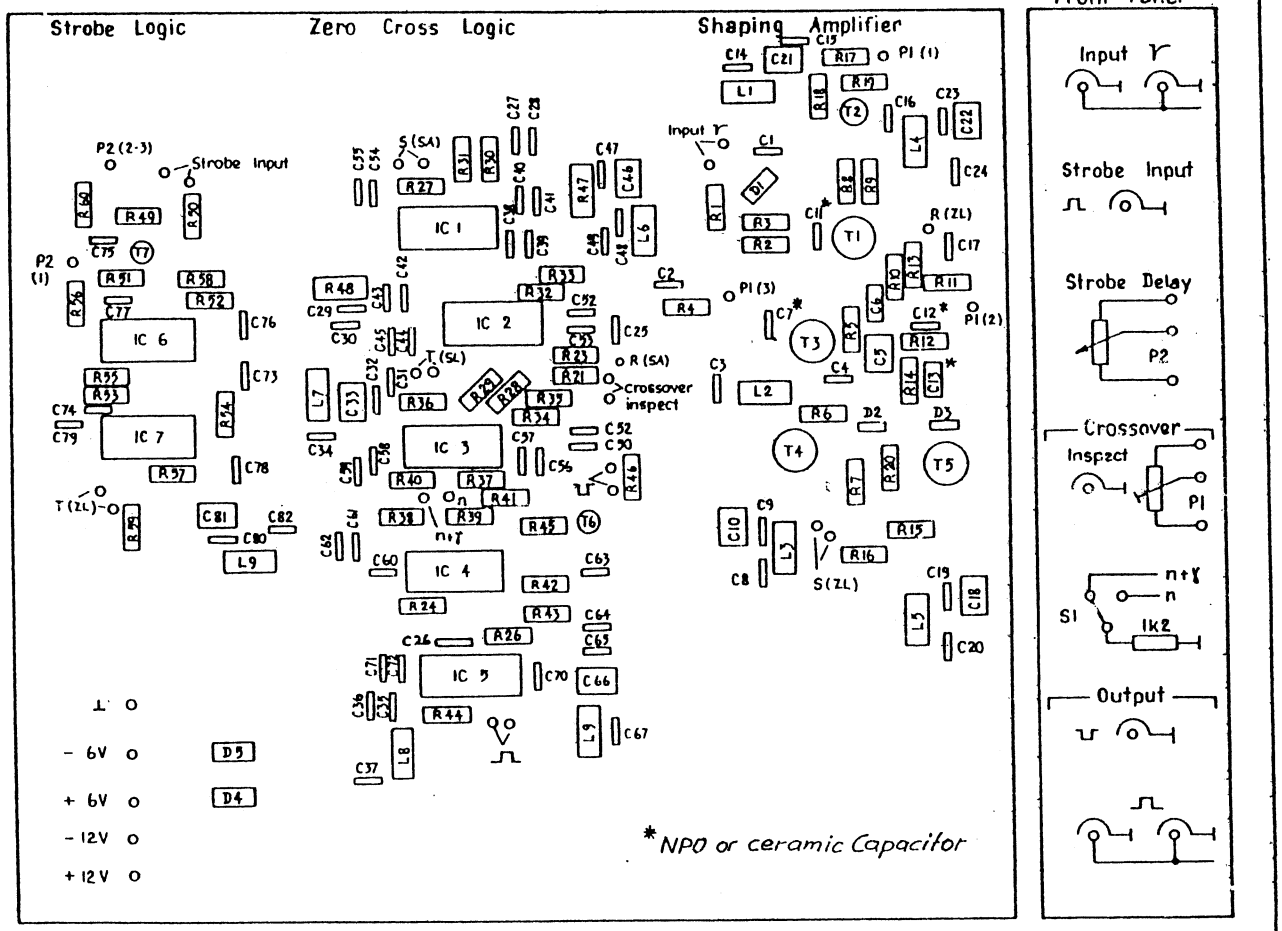

UNLESS OTHERWISE SPECIFIED	
TOLERANCES	REMOVE BURRS, BREAK SHARP EDGES & CORNERS
DECIMAL: ONE PLACE, TWO PLACE, THREE PLACE	MATERIAL
ANGULAR	FINISH
HOLES: .250 & UNDER +.003 -.001; OVER .250 +.005 -.001	
FLATNESS: .010 MAX PER LINEAR FOOT	

USED ON

		DATE
DRAWN	SAS	8/30/83
CHKD		
APPD MECH		
APPD ELEC		
NEXT ASSY	P/L A-20176	

COMP. ASS'Y

PULSE SHAPE DISCRIMINATOR

MODEL 2160A

DRAWING NO. B-20177 REV.

SCALE — DO NOT TEMPLATE DRAWING — SHT 1 OF 1